Regionale Ozeanographie

06 – Wärme und Stoffhaushalt - Oberflächenflüsse

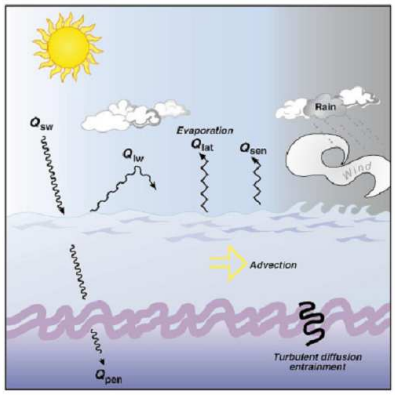

Literatur:

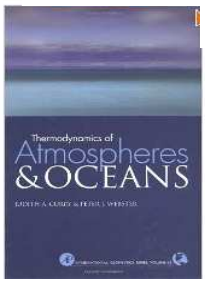

Curry, J.A. and P.J. Webster (1999) Thermodynamics of Atmospheres and Oceans, International Geophysics Series, Vol. 65, Academic Press.

Erhaltungsgleichungen

- continuity equation

$$\frac{D\rho}{Dt} = -\rho \nabla \cdot \boldsymbol{u} \quad , \quad \rho \frac{Dv}{Dt} = \nabla \cdot \boldsymbol{u}$$

- salt conservation equation

$$\rho \frac{DS}{Dt} = -\nabla \cdot \boldsymbol{J}_S = \nabla \cdot \kappa_S \nabla S$$

- conservative temperature equation

$$\rho \frac{D\Theta}{Dt} = -\nabla \cdot \boldsymbol{J}_\Theta + \text{very small source term} \approx \nabla \cdot \kappa_\Theta \nabla \Theta$$

- equation of state with conservative temperature as state variable

$$\rho = \rho(S, \Theta, p)$$

Budgets

$$DT/Dt = \partial T/\partial t + u\,\partial T/\partial x + v\,\partial T/\partial y + w\,\partial T/\partial z = Q_H/\rho c_p + \partial/\partial x(\kappa_H \partial T/\partial x) + \partial/\partial y(\kappa_H \partial T/\partial y) + \partial/\partial z(\kappa_V \partial T/\partial z)$$

zeitliche Variabilität
Advektion/Konvektion
Quellen/Senken
Mischung

plus
Randbedingungen

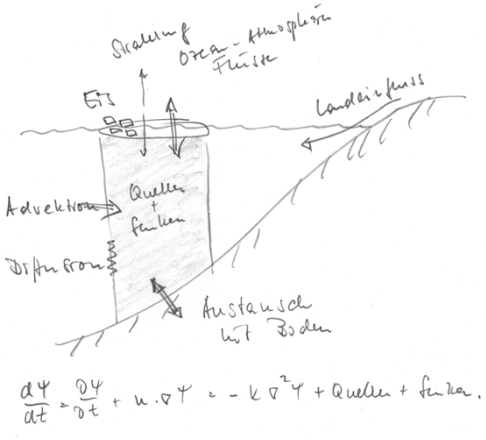

Ästuarine Zirkulation

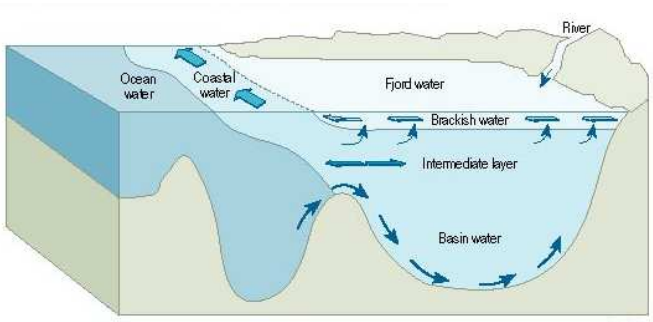

Volumenerhaltung (Volumenstransporte):

$V_{out} = V_{in}$ + Flusswasserzufuhr – Verdunstung + Niederschlag

Salzerhaltung: Salzmenge Einstrom = Salzmenge Ausstrom

$S_{out}\,\rho_{out}\,V_{out} = S_{in}\,\rho_{in}\,V_{in}$

Knudsens (1901) Formel, gilt unter stationären Verhältnissen

Süßwassertransporte in offenen Ozean

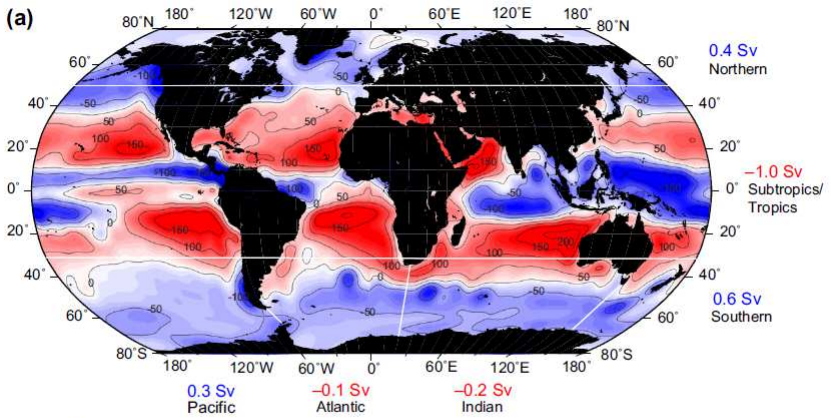

FIGURE 5.4 (a) Net evaporation and precipitation (E−P) (cm/yr) based on climatological annual mean data (1979–2005) from the National Center for Environmental Prediction. Net precipitation is negative (blue), net evaporation is positive (red). Overlain: freshwater transport divergences (Sverdrups or 1×10^9 kg/sec) based on ocean velocity and salinity observations. *Source: After Talley (2008).*

Süßwassertransporte in offenen Ozean

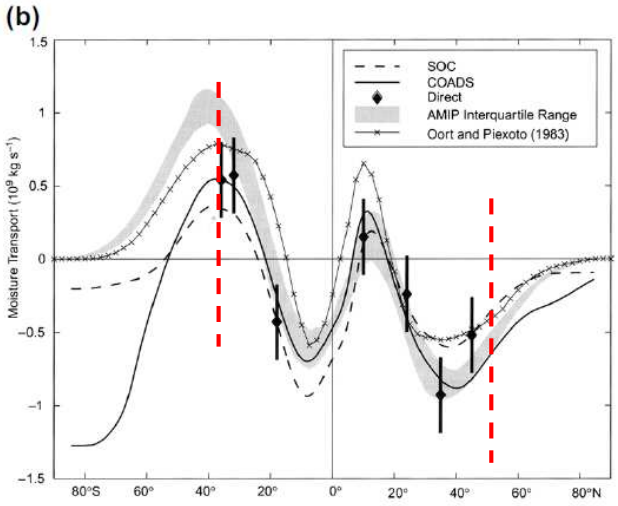

Wijffels (2001)

Oberflächen Salzgehalt

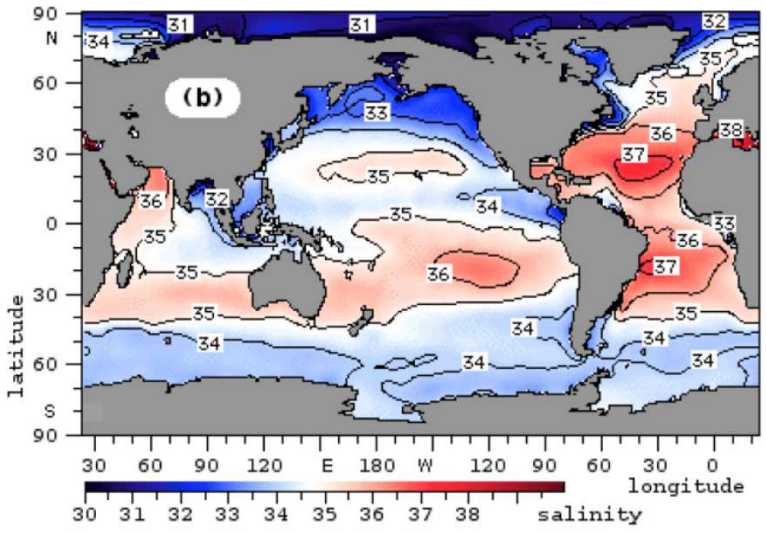

Tomczak & Godfrey, 2004

Oberflächentemperatur

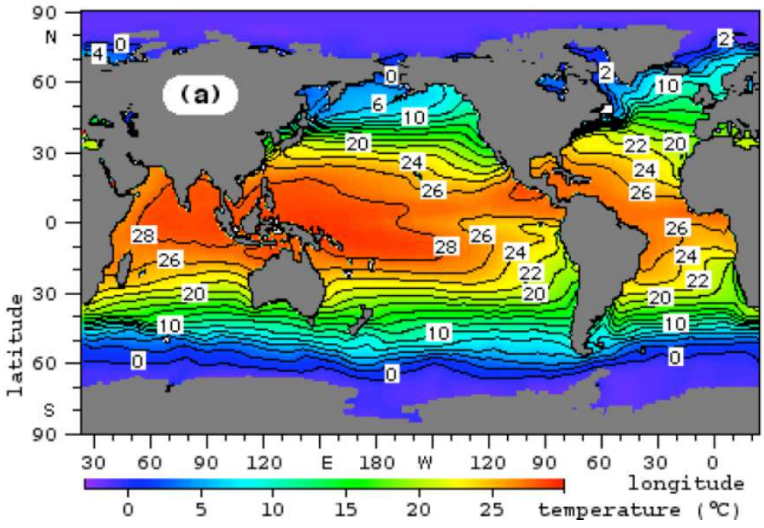

Tomczak & Godfrey, 2004

Oberflächenflüsse

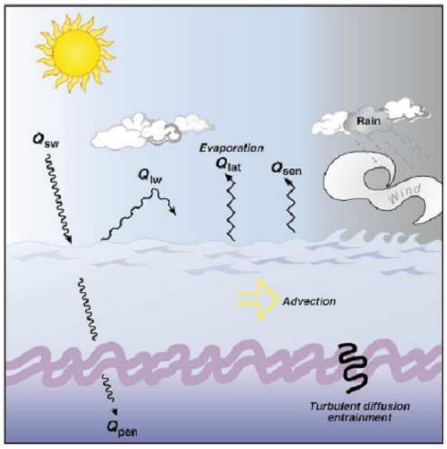

Wärmeflüsse

Süßwasserflüsse

Impulsflüsse

Spectral distribution of blackbody emissions

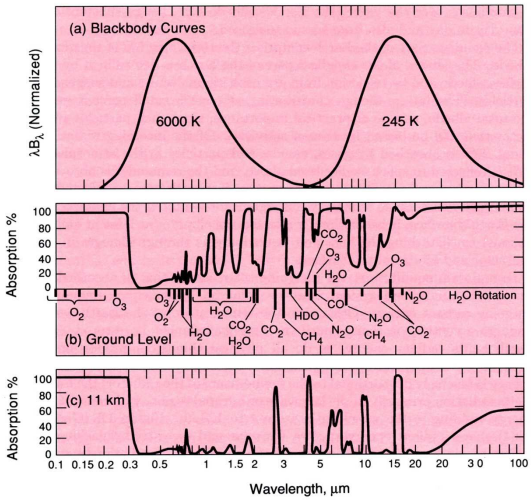

Fig. 1.1 (a) Spectral distribution of longwave emission from blackbodies at 6,000 K and 245 K, corresponding approximately to the mean emitting temperatures of the Sun and Earth, respectively, and (b) atmospheric absorption spectrum for a beam of radiation reaching the ground; (c) the same for a beam reaching the tropopause in temperate latitudes. Notice the comparatively weak absorption of the solar spectrum and the region of weak absorption from 8 to 12 μm in the longwave spectrum.

Schneider, 1992

Radiation energy balance

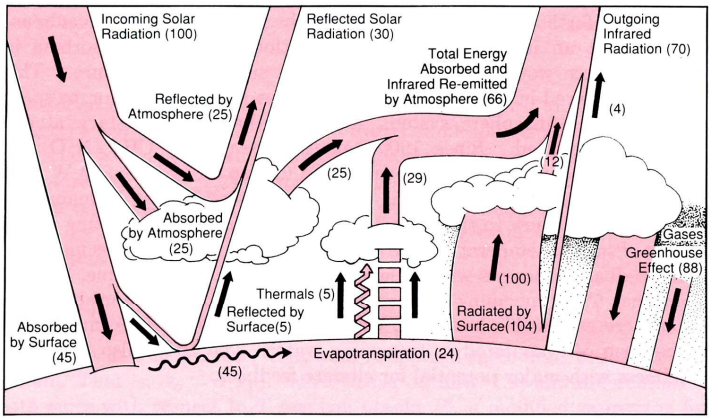

Fig. 1.2 The Earth's radiation energy balance, which controls the way the greenhouse effect works, can be seen graphically here. The numbers in parentheses represent energy as a percentage of the average solar constant – about 340 W m^{-2} – at the top of the atmosphere. Note that nearly half the incoming solar radiation penetrates the clouds and greenhouse gases to the Earth's surface. These gases and clouds re-radiate most (i.e., 88 units) of the absorbed energy back down toward the surface. This is the mechanism of the greenhouse effect.

Schneider, 1992

Attenuation and Dispersion

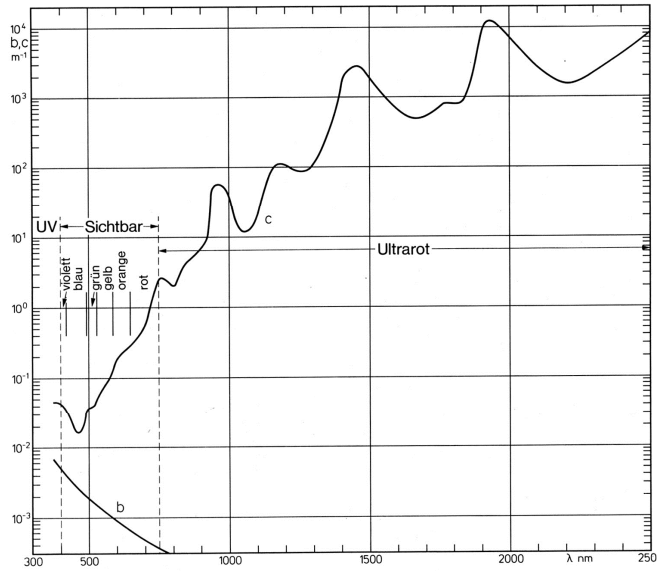

Abb. 2.21. Attenuationskoeffizient c und Streukoeffizient b für reines Wasser in Abhängigkeit von der Wellenlänge λ der Strahlung.

Dietrich et al., 1975

Shortwave radiation

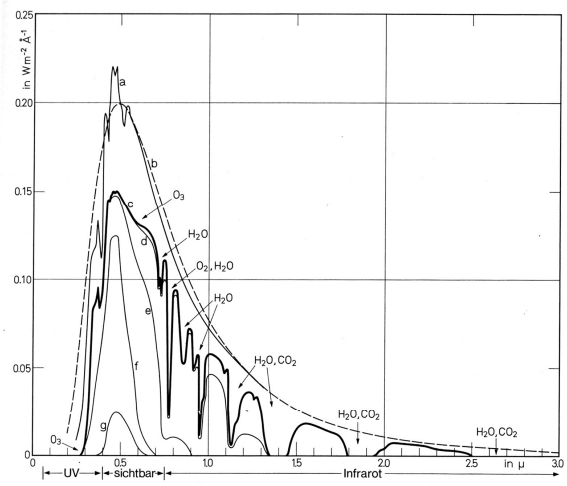

Abb. 4.10. Spektrale Energieverteilung zwischen Wellenlängen von 0,4 bis 3,0 μ bei senkrecht einfallender Sonnenstrahlung (angegeben in Watt pro Quadratmeter für Intervalle der Wellenlänge von 1 Ångström: $W\,m^{-2}Å^{-1}$), (Solarkonstante: 1396 $W\,m^{-2}$ = 2,00 cal $cm^{-2}\,min^{-1}$): a) Am Außenrand der Erdatmosphäre; b) für einen schwarzen Strahler von 5900° K; c) im Meeresniveau unter Hinweis auf die Absorption atmosphärischer Bestandteile: O_3, O_2, H_2O und CO_2; d) in 1 cm, e) in 1 m, f) in 10 m und g) in 100 m Wassertiefe.
a)–c): nach GAST (1965). d)–g): berechnet aus Kurve C mit Attenuationswerten für reines Meerwasser nach JERLOV (1968).

Dietrich et al., 1975

Cloud cover

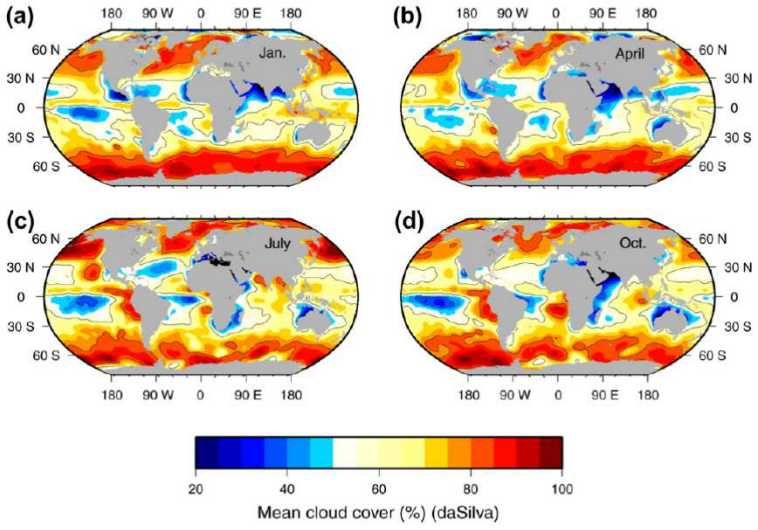

da Silva et al., 1994

Solar radiation at sea surface

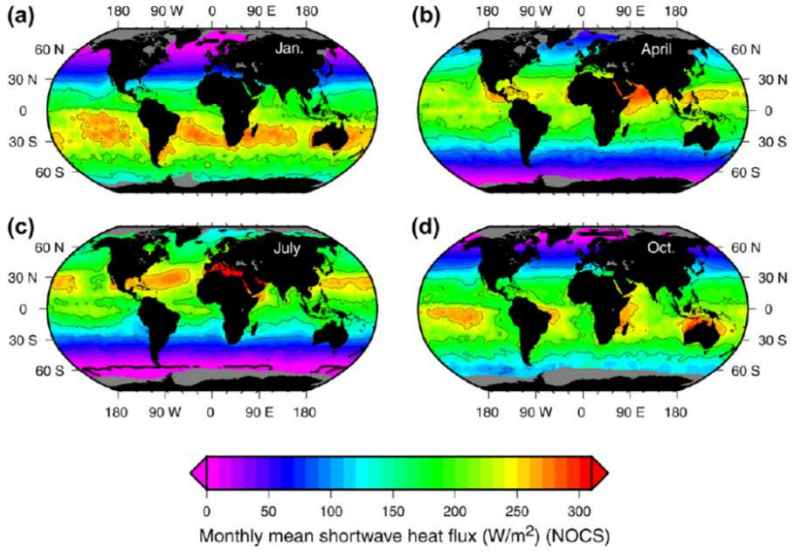

Grist & Josey, 2003

Energiebilanzen - Klima

Einkommende Strahlung

$Q_{in} = S * \cos \varphi$

Ausgehende Strahlung

$Q_{out} = \sigma * T^4$

Polewärtiger Wärmefluss

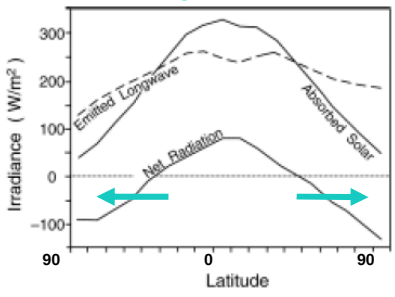

16

Strahlungsbilanz

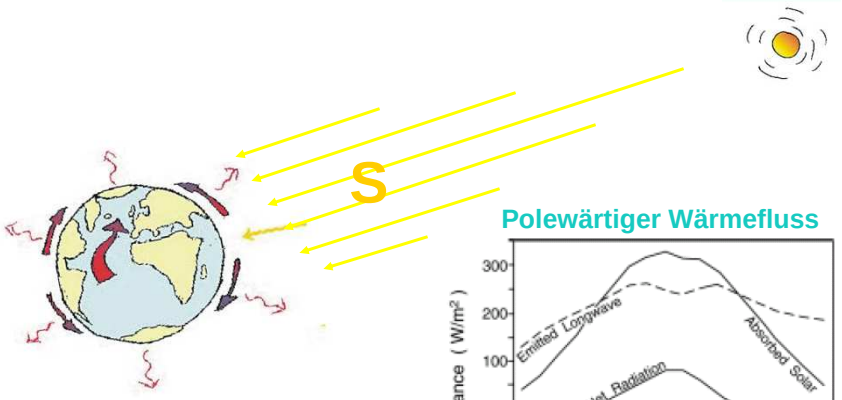

Einkommende Strahlung

$Q_{in} = S * \cos \varphi$

Ausgehende Strahlung

$Q_{out} = \sigma * T^4$

Polewärtiger Wärmefluss

Longwave radiation at sea surface

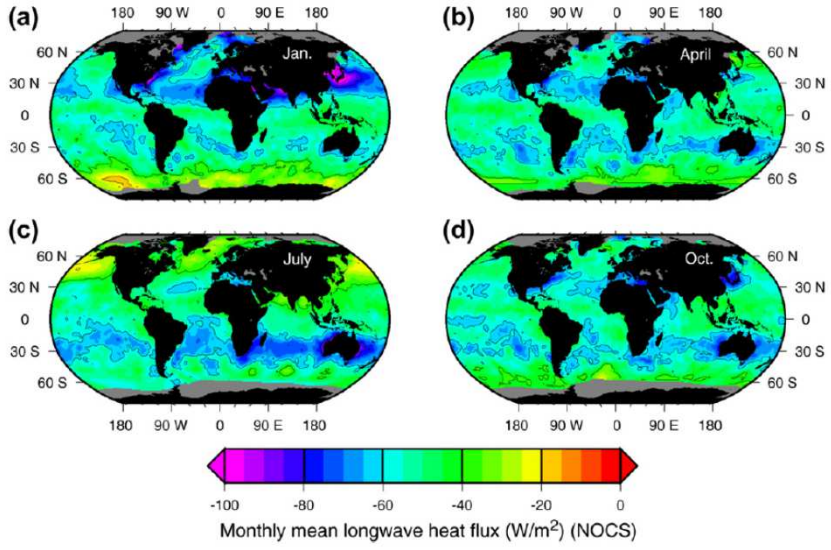

Grist & Josey, 2003

Sensible heat flux

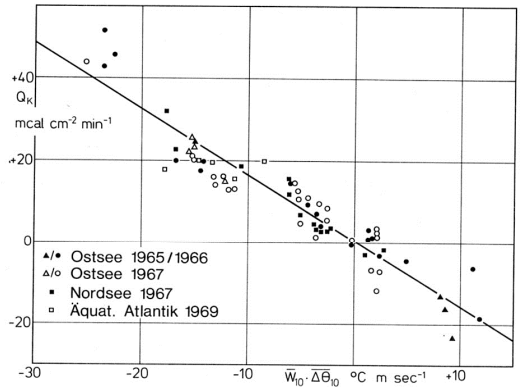

Abb. 4.06. Vertikalströme der sensiblen Wärme Q_K über See als Funktion des Produktes $W_{10} \cdot \overline{\Delta\Theta}_{10}$. W_{10}: Windgeschwindigkeit in m sec^{-1} in 10 m Höhe; $\overline{\Delta\Theta}_{10}$: Differenz der potentiellen Lufttemperatur in 10 m Höhe und der Wassertemperatur in°C; $Q_K > O$: Wärmestrom nach oben; ausgezogene Linie: Ausgleichsgerade. (Nach BROCKS, HASSE, KRUSPE, CLAUSS et al., aus KRUSPE, 1972).

Dietrich et al., 1975

Sensible heat flux

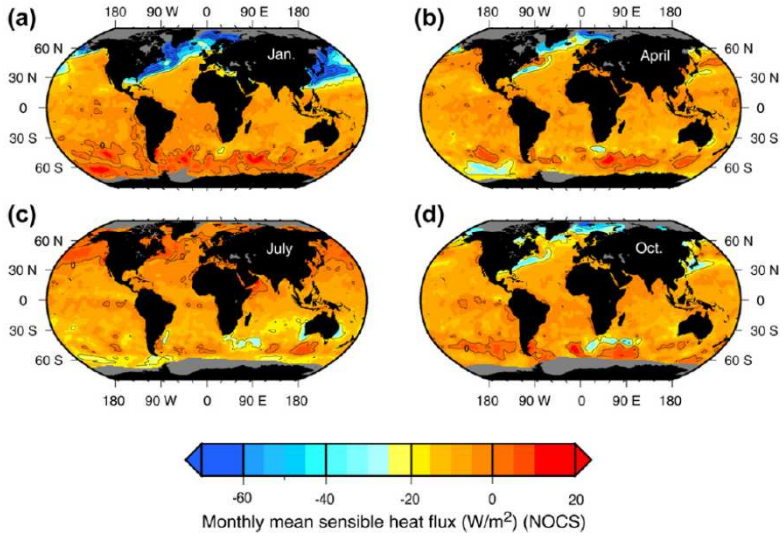

Grist & Josey, 2003

Evaporation

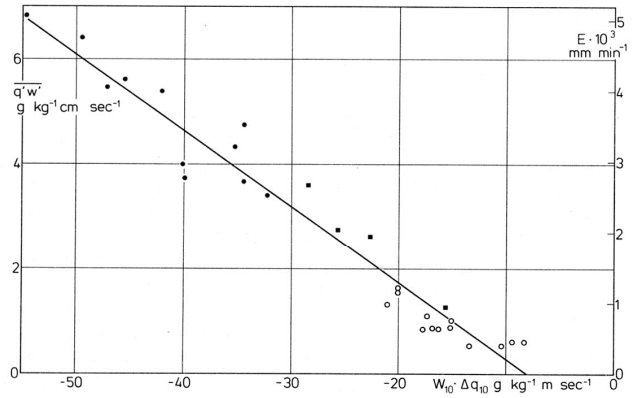

Abb. 4.07. Vertikalströme der Luftfeuchte (maritime Verdunstung) $\overline{q'w'}$ oder E als Funktion des Produktes Windgeschwindigkeit W_{10} in 10 m Höhe und der Feuchtedifferenz Δq_{10} Luft-Wasser (nach KRUSPE, 1972). Kreise: KRUSPE aus der Nordsee; Punkte: PHELPS aus dem tropischen Atlantik; Quadrate: PHELPS aus kalifornischen Gewässern; Ausgleichsgerade: ausgezogene Linie.

Dietrich et al., 1975

Latent heat flux

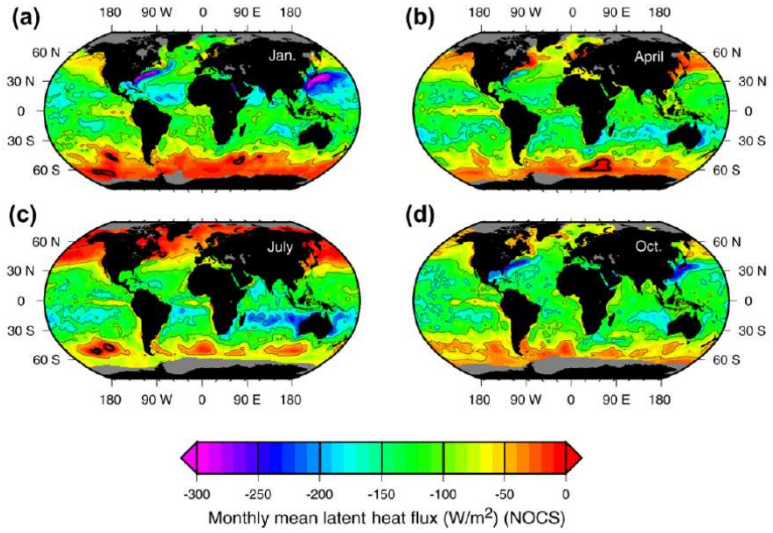

Grist & Josey, 2003

Evaporation & precipitation

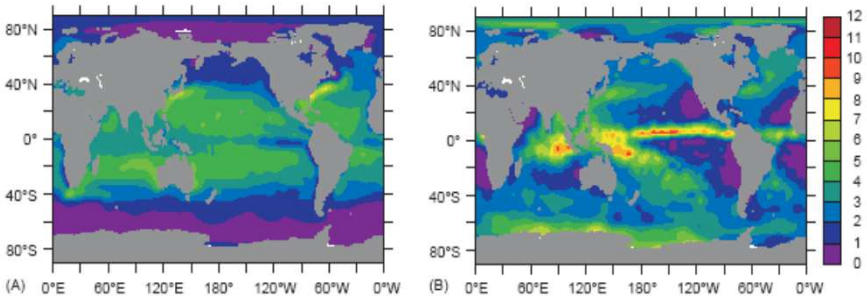

Figure 3 Mean climatologies of (A) evaporation, and (B) precipitation from da Silva *et al.* (1994). Both have units mm day^{-1} and share the scale shown on the right.

Net heat flux

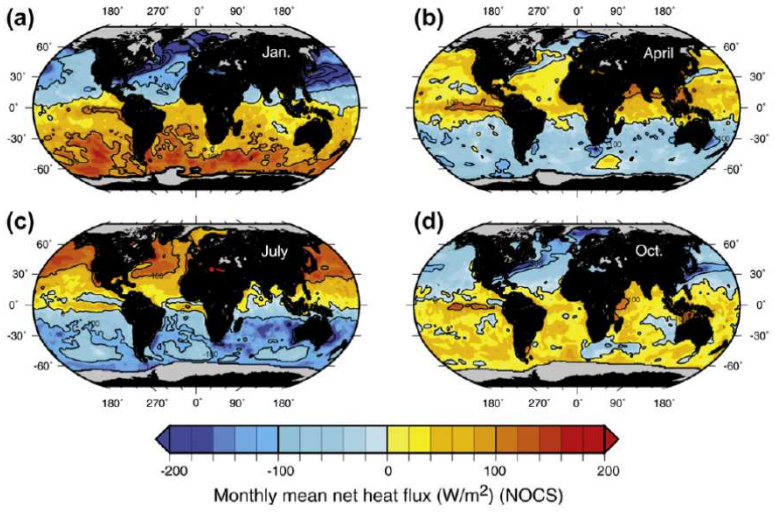

Grist & Josey, 2003

Annual mean net heat flux

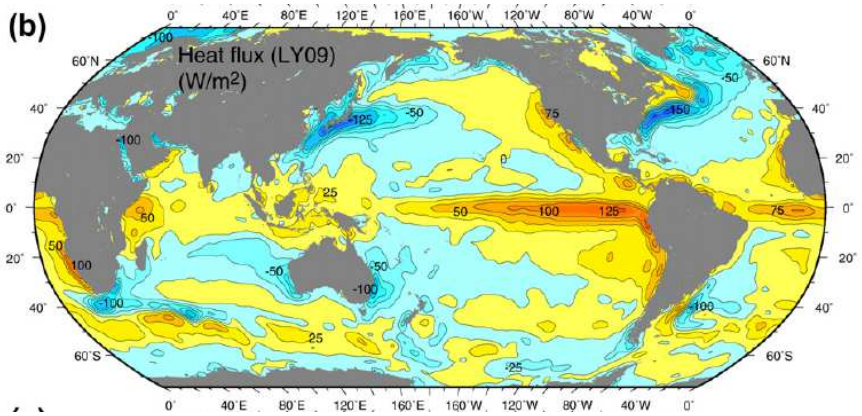

Large & Yeager, 2009

Annual mean net freshwater flux

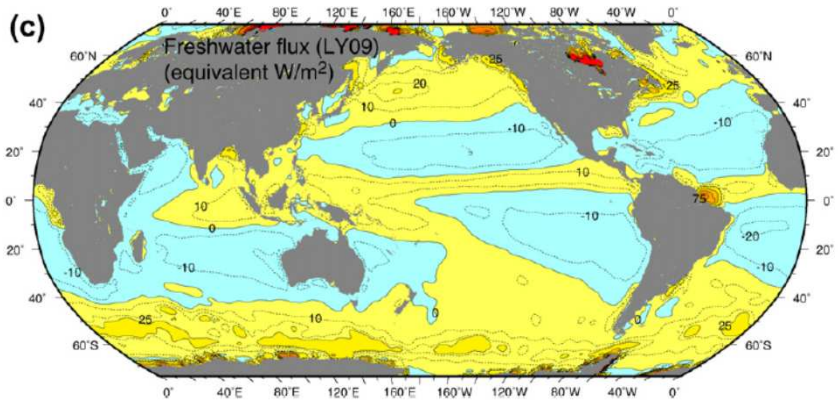

Large & Yeager, 2009

Annual mean net buoyancy flux

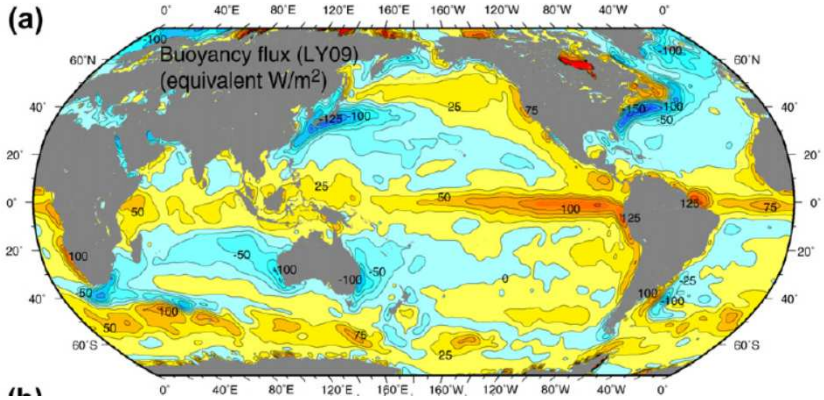

Large & Yeager, 2009

Air-Sea flux climatologies

Table 6.2.1 Surface flux estimates used in this study. Surface latent heating rates were converted to an equivalent evaporative water flux (E) using the latent heat of vaporization at the appropriate seasonal sea surface temperature taken from Levitus and Boyer (1994a). Baumgartner and Reichel (1975) only provide zonal flux integrals and thus is not used in Figures 6.2.1–6.2.3. In three data sets runoff R is also available.

Source	Type	Parameters	Temporal coverage
Surface observations (SOC)	Josey *et al.* (1996)	E, P	Climatology
Surface observations (COADS)	da Silva *et al.* (1994)	E, P	Climatology
Surface observations	Baumgartner and Reichel, (1975) [not gridded]	E–P, R	Climatology
Surface observations	Esbensen and Kushnir (1981)	E	Climatology
Surface observations	Oberhuber (1988)	E,P	Climatology
Blended satellite and surface observations	Legates and Wilmott (1990)	P	1979–96
Surface observations	Jaeger (1983)	P	Climatology
Blended satellite and surface observations and model output	Xie and Arkin (1997)	P	1979–98
Blended satellite and surface observations (Limb90/MSU)	Tod Mitchell, personal communication (1999)	P	1979–92
Satellite observations	Jourdan *et al.* (1997)	E–P	Climatology
Atmospheric re-analysis (ECMWF)	Keith (1995)	E–P, R	1989
Atmospheric re-analysis (ECMWF)	Barnier *et al.* (1995)	E	1986–88
Atmospheric re-analysis (NCEP)	Trenberth and Guillemot (1998)	E–P	1979–95
Atmospheric re-analysis (NCEP)	Kalnay *et al.* (1996)	E, P, R	Climatology

HOAPS: www.hoaps.zmaw.de

Wijffels, 2001

Mean E-P fluxes

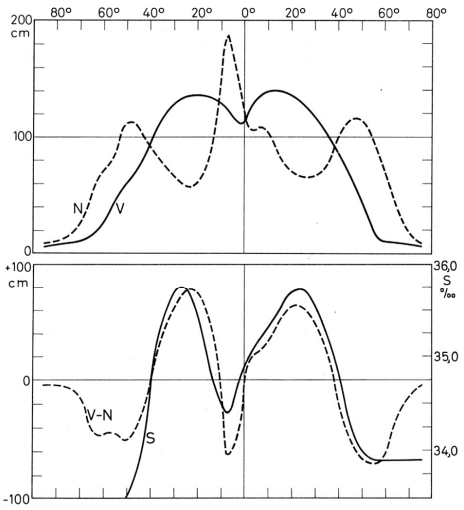

Abb. 4.17. Meridionale Verteilung von Niederschlag N und Verdunstung V (oben) sowie $V–N$ und Salzgehalt S (unten) an der Oberfläche des Weltmeeres einschließlich der Nebenmeere im zonalen Jahresmittel (nach WÜST, 1954).

Dietrich et al., 1975

River run-off

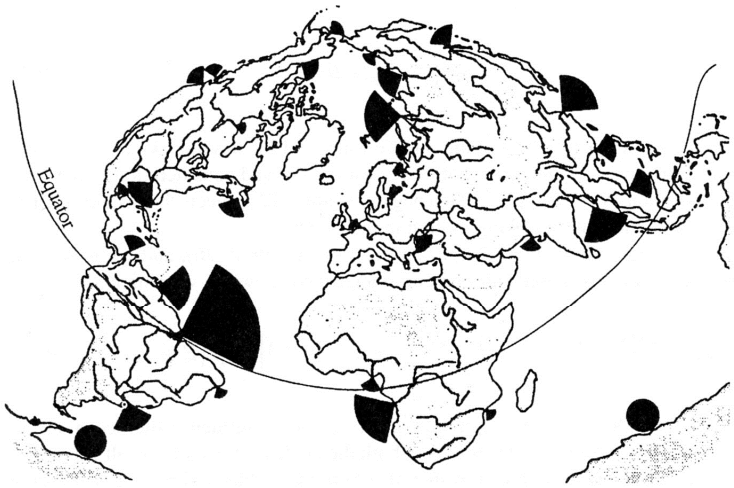

Figure 9.6 Global river runoff. Segment areas are proportional to the annual volume flow. Most of the runoff occurs in the Northern Hemisphere because of its greater land mass. The largest volume of fresh-water input comes from the Amazon River. Circles on the coast of Antarctica indicate runoff from glaciers. (From Woods, 1984.)

River run-off

Tabelle 4.05 Festländischer Abfluß im Jahresmittel in 10^3 m^3 sec^{-1} (nach MARCINEK, 1964) mit mehr als $2{,}0 \times 10^3$ m^3 sec^{-1}, geordnet nach Ozeanen (Grenzen Tafel 1).

Atlantischer Ozean	10^3 m^3 sec^{-1}	Pazifischer Ozean	10^3 m^3 sec^{-1}
Amazonas	180,0	Jangtse	34,0
Kongo	42,0	Mekong	15,9
Orinoko	28,0	Amur	11,0
La Plata*	24,1	Sikiang	11,0
Mississippi	17,5	Columbia	6,7
Jenisey	17,4	Yukon	4,3
Lena	15,5	Fraser	3,9
Ob	12,5		
St.-Lorenz-Strom	10,4		
Magdalenenstrom	8,0	Indischer Ozean	10^3 m^3 sec^{-1}
MacKenzie	7,5		
Donau	6,5	Brahmaputra	20,0
Niger	5,8	Irawadi	14,0
Petschora	4,1	Indus	3,9
Kolyma	3,8	Sambesi	2,5
Dwina	3,5		
San Francisco	3,3		
Grijalva	3,3		
Newa	2,6		
Pyasina	2,6		
Nelson	2,3		
Rhein	2,2		

* Parana und Uruguay

Dietrich et al., 1975

Hydrological cycle

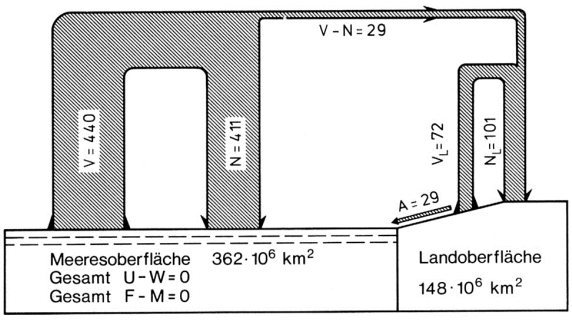

Abb. 4.18. Wasserumsatz auf der Erde in 10^3 km^3 Jahr^{-1}.

Dietrich et al., 1975

Young ice

Ice growth

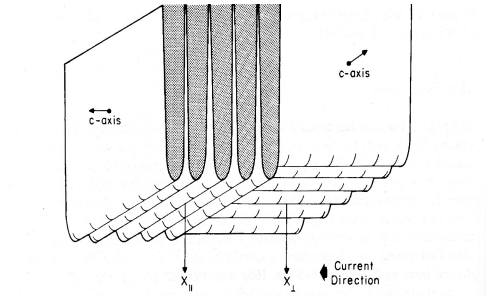

Figure 2.8. The shape of the interface in a growing ice sheet. Two crystals are shown, with differing c-axis orientations relative to the prevailing current (after Weeks and Gow, 1978).

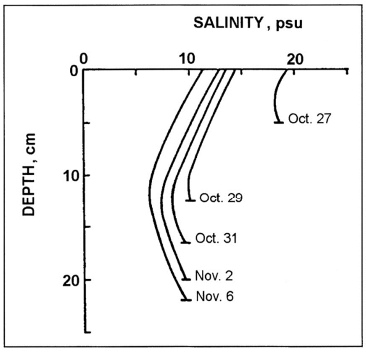

Figure 2.10. The rapid desalination of young ice (after Lewis, 1970).

Wadhams, 2002

Ice growth

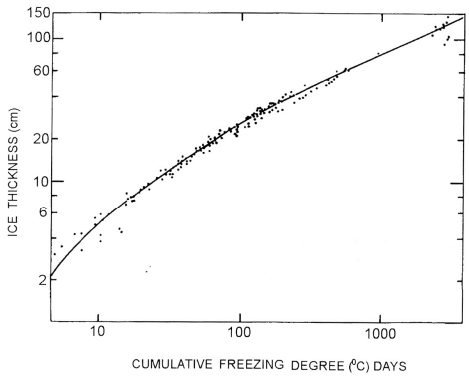

Figure 3.6. Anderson's (1961) relationship for young ice thickness as a function of degree-days of cold.

Wadhams, 2002

Ice growth

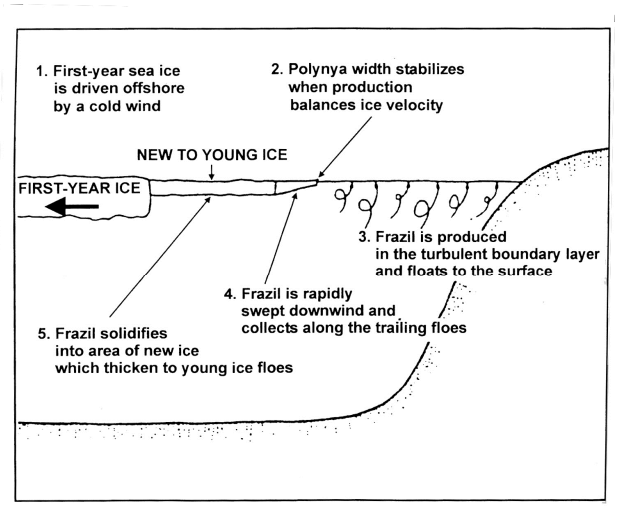

Figure 4.8. Simple dynamics of a wind-driven coastal polynya (after Pease, 1987).

Wadhams, 2002

Ice rafting

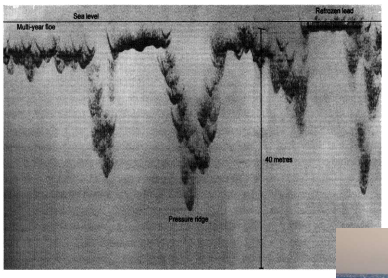

Figure 5.11. An under-ice sonar profile obtained by a submarine in the Arctic Ocean.

Wadhams, 2002

Seasonal ice

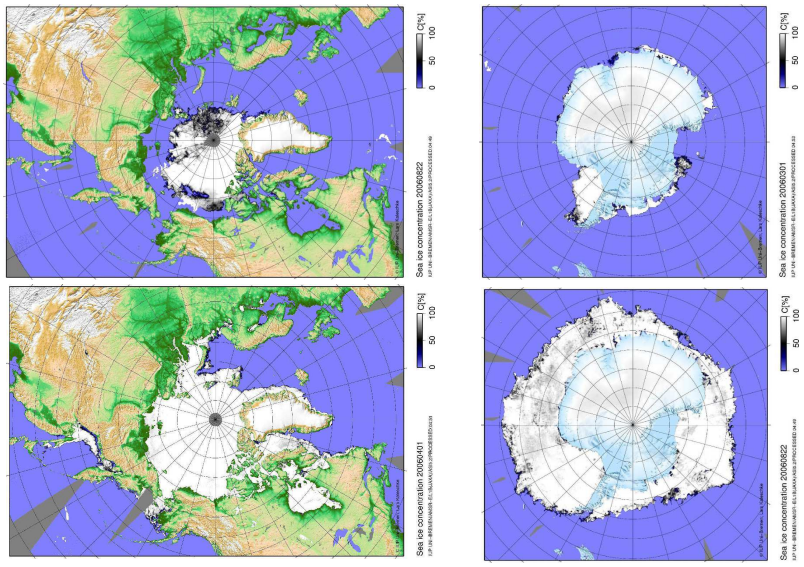

Seasonal ice

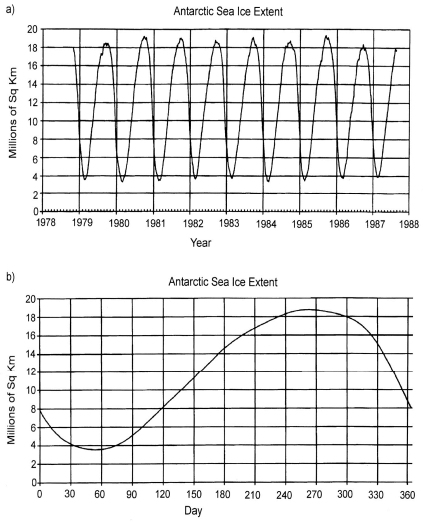

Figure 1.19. (a) The cycle of Antarctic sea ice extent, 1979–87. (b) Average seasonal cycle of ice extent in the Antarctic (after Gloersen *et al.*, 1992).

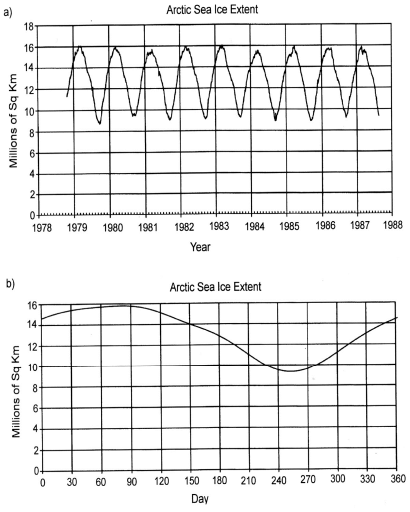

Figure 1.17. (a) The cycle of Arctic sea ice extent, 1979–87. (b) Average seasonal cycle of ice extent in the Arctic (after Gloersen *et al.*, 1992).

Wadhams, 2002

Wind drag coefficients

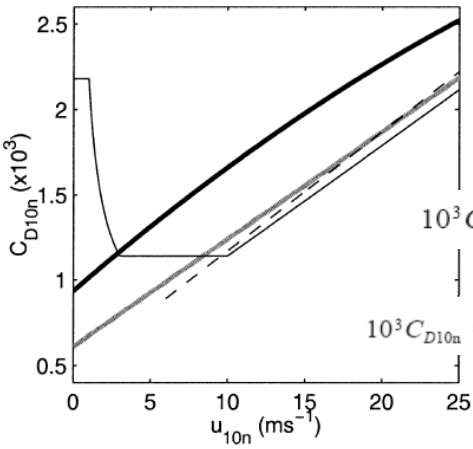

FIG. 1. Variation of the neutral drag coefficient C_{D10n} (multiplied by 10^3) with the 10-m neutral wind speed u_{10n}. Solid gray line: Smith (1980); dashed black line: Taylor and Yelland (2000); solid thick black line: HR; solid thin black line: UWM/COADS.

$$\tau_x = \rho C_D u_x (u_x^2 + u_y^2)^{1/2}$$
$$\tau_y = \rho C_D u_y (u_x^2 + u_y^2)^{1/2},$$

Smith, 1980

$$10^3 C_{D10n} = 0.61 + 0.063 u_{10n}.$$

Hellermann & Rosenstein, 1983

$$10^3 C_{D10n} = 0.934 + 0.0788u - 0.000616u^2,$$

Josey et al., JPO, 2002

Wind stress

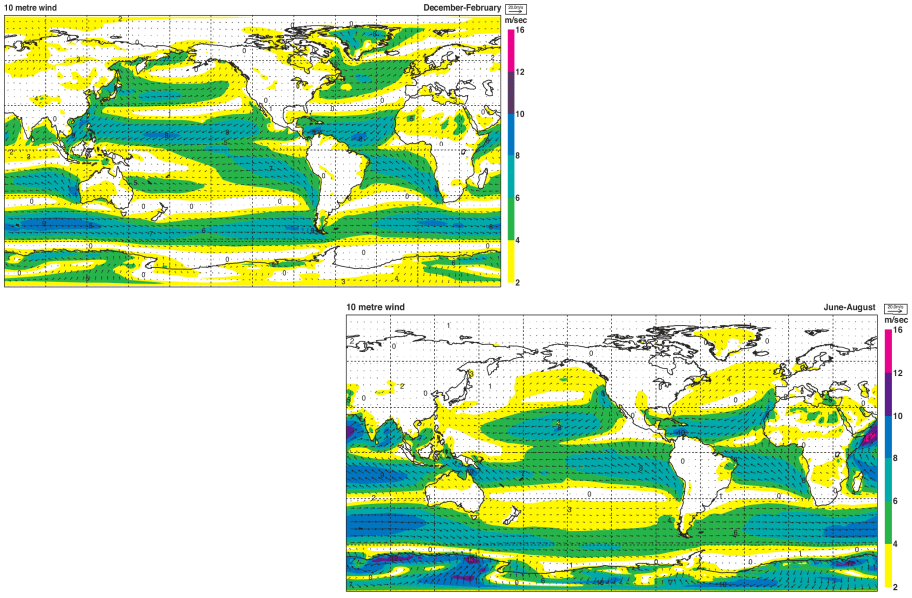

Wind stress and wind curl

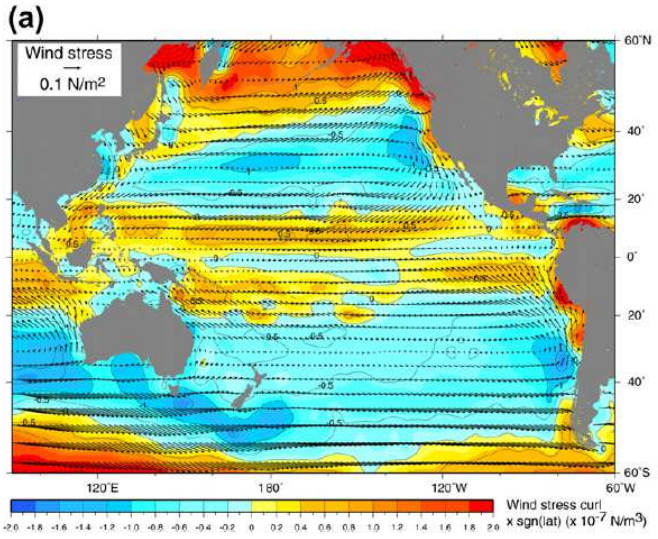

Kalnay et al, 1996

Wind stress and wind curl

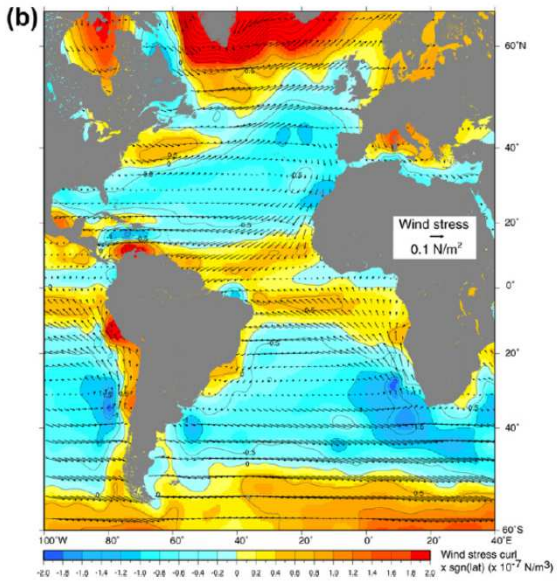

Kalnay et al, 1996

Wind stress and wind curl

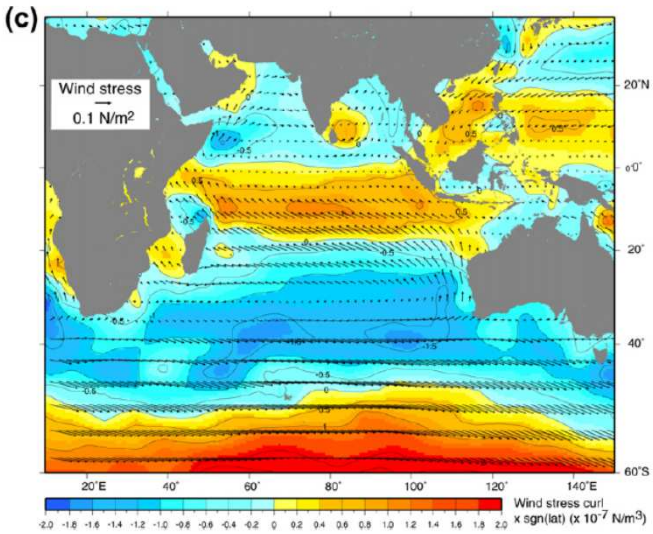

Kalnay et al, 1996

Zonal mean wind drag

Fig. 11f)

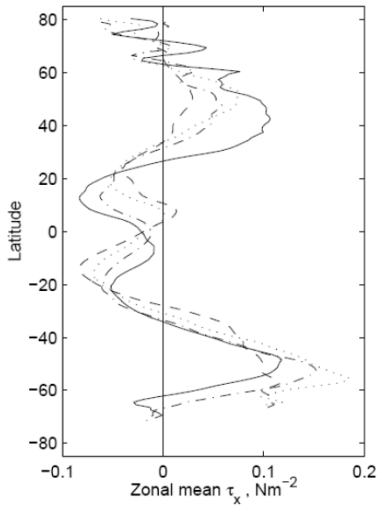

Fig. 11g)

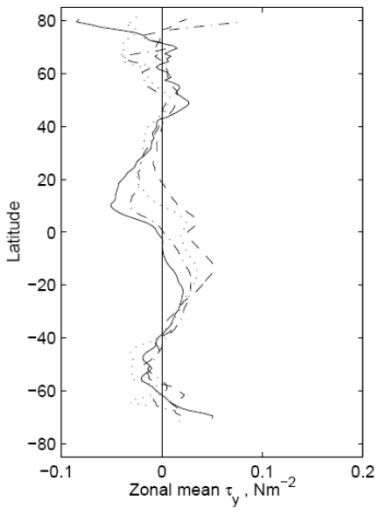

Sverdrup transport

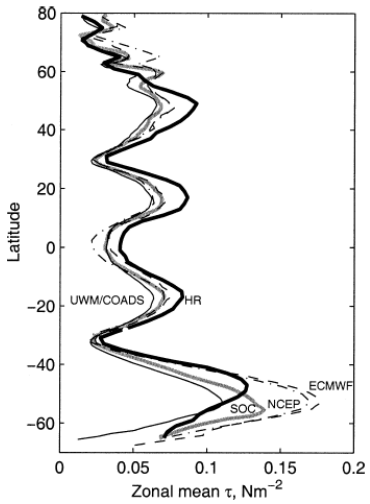

FIG. 5. Zonally averaged annual mean wind stress magnitude, units N m^{-2}. Solid gray line: SOC; solid thick black line: HR; solid thin black line: UWM/COADS; dashed black line: ECMWF; dash–dot line: NCEP–NCAR.

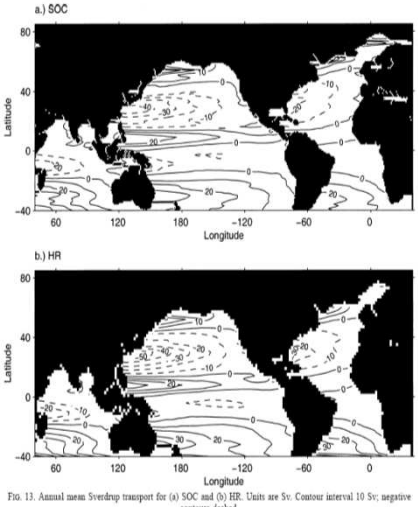

FIG. 13. Annual mean Sverdrup transport for (a) SOC and (b) HR. Units are Sv. Contour interval 10 Sv; negative contours dashed.

Josey et al., JPO, 2002